Bull. Mater. Sci., Vol. 40, No. 4, August 2017, pp. 667–682
DOI 10.1007/s12034-017-1422-0

Gas sensing behaviour of cerium oxide and magnesium aluminate composites

N NITHYAVATHY[1,2], V RAJENDRAN[2,3,*], L JOHN BERCHMANS[4], M MAAZA[3,5], S KRITHIKA[1] and S ARUNMETHA[2]

[1]Mechatronics Engineering, Kongu Engineering College, Perundurai, Erode 638052, India
[2]Centre for Nanoscience and Technology, K. S. Rangasamy College of Technology, Tiruchengode 637 215, India
[3]UNESCO-UNISA Africa Chair in Nanosciences - Nanotechnology, College of Graduate Studies, University of South Africa, Muckleneuk Ridge, P.O. 392, Pretoria, South Africa
[4]Electro-Pyrometallurgy Division, CSIR—Central Electrochemical Research Institute, Karaikudi 630006, India
[5]Nanosciences African Network (NANOAFNET), iThrmba LABS-National Research Foundation, Somerset West 7129, South Africa
*Author for correspondence (veerajendran@gmail.com)

MS received 11 February 2016; accepted 19 October 2016; published online 26 July 2017

Abstract. Composites of cerium oxide (CeO_2) and magnesium aluminate ($MgAl_2O_4$) were prepared by the molten salt synthesis (MSS) method at 1130 K. The composite samples were named as MA, MAC0.07 and MAC0.14 (at CeO_2: 0, 0.07 and 0.14 g in $MgAl_2O_4$, respectively) and these were characterized by X-ray diffraction and energy-dispersive X-ray analyses. It is seen that the microstructure of the composite samples are quite similar except for a small increase in particle size. The energy-dispersive X-ray analyses provide the presence of concentration of Ce, Mg, Al and O in the composite. Scanning electron microscope, coupled with energy-dispersive X-ray analysis (SEM-EDAX) was used to identify the morphology, microstructure and elemental composition of the prepared samples. The decomposition and dissociation reactions of the precursors were determined using differential thermal and thermogravimetric analysis (TGA). A lone pair of the electron state was identified from the electro paramagnetic resonance spectrum. An optical energy band gap of 3.3 eV was calculated from the UV–Vis absorbance spectra. The gas response to changes in oxygen (O_2), carbon monoxide (CO) (at 0.5, 1.0 and 1.5 bar) and ethanol (at 50 and 100 ppm) was quantitatively analysed in all the samples at different operating temperatures (300–500 K). The magnitude of the temperature varied linearly regardless of the gas pressure inside the chamber, by increasing the supply in the heating pad, mounted below the sensor sample. The composite samples indicate a good response to different gases with detection of the smallest change in gas pressure.

Keywords. Composite; molten salt synthesis; thermogravimetric analysis; paramagnetic behaviour; gas sensor response.

1. Introduction

A small-sized gas sensor with a low operating temperature semiconductor is designed to meet the recent demands of gas sensors [1,2]. In general, a semiconductor gas sensor shows good sensitivity, stability and selectivity in gas detection [3]. The semiconductor metal oxides, such as tin oxide, titanium oxide, cerium oxide (CeO_2), zinc oxide, zirconium oxide and tungsten oxide are used as sensing materials for gas sensors [4,5]. Generally, gases such as nitric oxide (NO), nitrogen dioxide, carbon monoxide (CO), carbon dioxide (CO_2), hydrogen sulfide, sulfur dioxide, ozone, ammonia and organic gases such as methane, propane, liquid petroleum gas, etc., are to be deducted for both industry and household applications [6,7].

Magnesium aluminate ($MgAl_2O_4$), a spinel cubic structure, with a general formula AB_2O_4, where A represents a divalent metal ion such as magnesium, iron, nickel, manganese and/or zinc; B represents a trivalent metal ion such as aluminium, iron, chromium or manganese and O represents the oxygen (O_2) states [8–10]. In $MgAl_2O_4$ spinel, the Mg^{2+} cation fills the tetrahedral sites and the Al^{3+} cation reside in the octahedral positions. It is an insulating material with a low thermal expansion coefficient, resistance to neutron irradiation, possess low di-electric loss, high-mechanical strength, chemical inertness, wide band gap, low density, high-melting point and high-thermal shock resistance [11,12]. $MgAl_2O_4$ is used for different applications, such as humidity sensors, dielectric, catalyst support, reinforcing fibres, photoluminescent and ceramic pigments [11,13]. In turn, these applications require a small concentration of additives and high pressure-assisted sintering [14,15].

Cerium (IV) oxide or ceria, a face-centred cubic crystal, is a rare earth oxide material and is used in applications like catalyst, ultraviolet (UV) filtration and chemical and mechanical polishing. It has currently attracted great interest in exhaust

gas sensing and in promoting the oxidation of CO and hydrocarbon [16]. It is an n-type semiconducting metal oxide used as an O_2 storage substance [17,18]. CeO_2 is a promising material used for sensing O_2 at high temperatures owing to its chemical stability and high diffusion coefficient vacancies.

Owing to a large number of lattice defects and O_2 vacancies, a noteworthy enhancement and potential catalytic activity of CeO_2 is observed. By partial substitution or doping the cerium atoms with other metal atoms of lower oxidation state, the number of defects is increased [19,20]. In turn, CeO_2 shows improved gas sensing properties when combined with different cation dopants, such as Mg, Al, Zr, Nd, Ca, Pb, Mn, Cu, Zn, Co, Y, Ba and Sr. The main feature of O_2 vacancy in CeO_2 includes its dependency on size and chemical mobility.

Different methods, such as chemical vapour deposition, chemical gas phase growth, sol–gel processing and molecular beam epitaxial, molten flux and plasma synthesis are used to synthesize nano-sized metal oxide particles [21,22]. In this experiment, different physical and chemical synthesis techniques are used to prepare a CeO_2 thin sensor sample. However, these synthesis techniques require high vacuum and high-purity precursor materials. On the other hand, molten salt synthesis (MSS) technique is found to be simple, cost effective and can be used to prepare a dense powder sample with better optical quality. The MSS technique is generally used to prepare the Ce and $MgAl_2O_4$ composite materials while the same cannot be prepared by using other conventional methods for gas sensing.

Today, a gas sensor should be designed such that it works under certain critical conditions both in low and higher operating temperatures. Moreover, the applications of CeO_2 and $MgAl_2O_4$ composites on gas sensing at different operating temperatures and pressures are found to be scanty. The molten flux method is used to prepare the CeO_2 and $MgAl_2O_4$ composite materials. However, to our knowledge, no work has been done on CeO_2 incorporated in $MgAl_2O_4$ as compared with CO_2 and ethanol gas sensors at room temperature as well as at elevated temperatures. These nano-structured materials are used for sensing the gases such as ethanol and tri-methylamine.

This study deals with the synthesis and characterization of CeO_2 and $MgAl_2O_4$ composites prepared by the molten salt/flux synthesis method at 1130 K. Sodium chloride (NaCl) and potassium chloride (KCl) were used as the flux to prepare a composite sample of CeO_2 and $MgAl_2O_4$. The sample was used in sensing O_2, CO and ethanol (C_2H_5OH) at different operating temperatures (300, 400 and 500 K). The changes in the resistance, sensor response and response/recovery time were analysed for different concentrations of CeO_2 and $MgAl_2O_4$ composites.

2. Materials and methods

The different compositions of CeO_2 and $MgAl_2O_4$ composites were prepared by the MSS method. Chemicals such as magnesium oxide (MgO), aluminium oxide (Al_2O_3), CeO_2, NaCl, KCl, hydrochloric acid (HCl) and ethanol were used as raw materials for the synthesis. All the chemicals used in this study were of analytical grade and weighted according to the stoichiometric compositions using a digital balance (CP225D; Sartorius, Goettingen, Germany). The stirring process was conducted by using a magnetic stirrer (G1631; Elico, USA). The mechanical grinding of the composites was carried out by a ball mill (Ball Mill PM100; Retsch, Haan, Germany) and the pellet was prepared by a pellet press (SRNO 833; Hydraulic Pellet Press, USA). The value of resistance (R) of the sensor samples was calculated using a digital micro-ohmmeter (53C; Agronic, Mumbai, India).

2.1 *Synthesis of CeO_2 and $MgAl_2O_4$ composites by molten salt synthesis*

Generally, two reactions were considered for the formation of composites in the molten salt synthesis. In the first reaction, the reactants (MgO, Al_2O_3 and CeO_2) were dissolved in the molten salt (NaCl and KCl) and a mixture was formed. In the second sequence, one of the reactants was dissolved in the molten salt, and the dissolving component was transported to the outer surface of the other reactant. Initially, a mixture of the reactants and salt was heated above the melting temperature of the salt (at 1130 K for 8 h) and a mixture of the reactants was formed. This mixture was then mixed in molten salt to obtain a uniform mixture. The characteristics of the mixture such as particle size and shape were controlled by varying the temperature and duration of the heating [21].

Then, to obtain the composite powder, the mixture was cooled at room temperature and washed with an appropriate solvent (double distilled water) to remove the salt. Finally, the samples of the $MgAl_2O_4$ composites with two different concentrations of $x(CeO_2)$ (with $x = 0.07$ and 0.14 g) were termed as MAC0.07 and MAC0.14, respectively. The samples were dried separately below 400 K for 24 h and cooled at room temperature. From the earlier studies [21], it was observed that the response of sensors increases with increasing the quantity of CeO_2 concentration up to 4%. However, the response decreases with further CeO_2 additions up to 6%. In this study, CeO_2 concentration additions on $MgAl_2O_4$ up to 0.14 g promoted the gas reaction in the form of a catalyst, improving surface reactions towards different gases. On further increasing the concentration of CeO_2, there was a reduction in the available adsorption sites on the surface, thus, leading to the decrease in the sensor response. Hence, addition of CeO_2 concentrations of 0.07 and 0.14 g were considered for conducting further experiments.

2.2 *Synthesis of $MgAl_2O_4$ sample*

A similar procedure was conducted in the preparation of $MgAl_2O_4$ using MSS. MgO and Al_2O_3 were used to prepare the sensor sample; NaCl and KCl were used as the flux salts. The resulting mixture was then ground and washed with hot

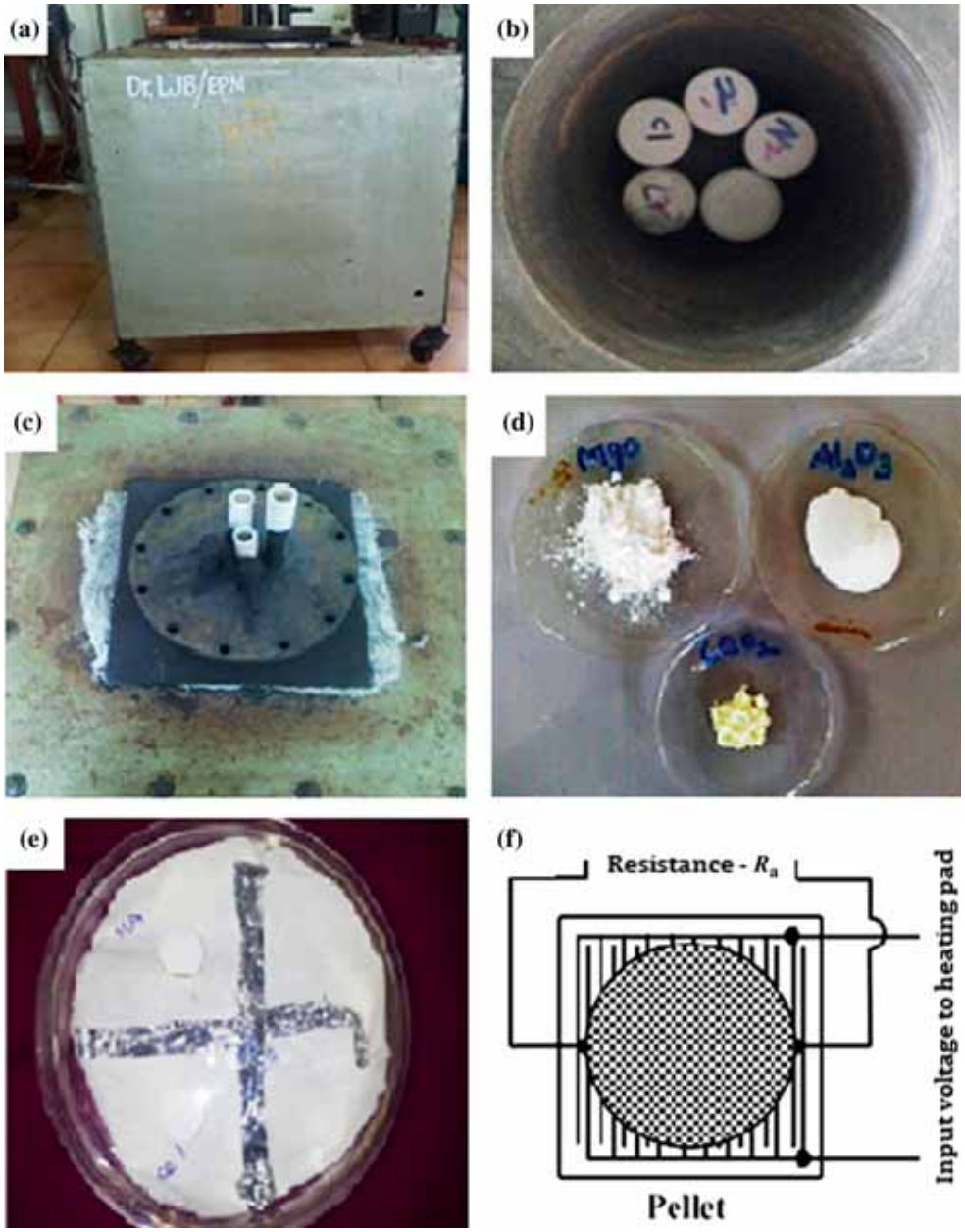

Figure 1. Different stages of CeO_2 and $MgAl_2O_4$ composite—molten flux synthesis: (**a**) electric resistance furnace, (**b**) inner view of furnace, (**c**) crucible location, (**d**) sample powder, (**e**) sample pellet and (**f**) heating pad.

distilled water followed by the addition of 5% HCl to obtain a powder, which was further washed with hot distilled water two more times. Finally, the $MgAl_2O_4$ powder was obtained and termed as MA.

2.3 *Characterization*

The structural and functional properties of MA, MAC0.07 and MAC0.14 were characterized by using X-ray diffraction (XRD; X'Pert PRO; PAN analytical, Almelo, the Netherlands) and Fourier transform-infrared spectroscopy (FTIR; Spectrum 100; Perkin Elmer, Shelton, CT, USA). Thermogravimetric analysis (TGA) was used to calculate the mass change of the prepared samples in a controlled atmosphere. Differential thermal analysis (DTA) was used to assess the difference in temperature of the sample when compared with a reference. Electron paramagnetic resonance (EPR) spectroscopy was used as a sensitive and specific method for studying the radicals formed in chemical reactions using a microwave frequency of 9.8 GHz with fields of 6500 G sweep width (EPR Spectrometer; Bruker Bio Spin GmbH, Rheinstetten, Germany). Subsequently, repeated tests were conducted

on all the samples individually inside the sensing chamber. The scanning electron microscope, coupled with energy-dispersive X-ray analysis (SEM-EDAX; JSM 6400; JEOL, Japan), was used to identify the morphology, microstructure and elemental composition of the prepared samples.

Initially, 100 mg sample powder (e.g., MA) was mixed with a polyvinyl alcohol (PVA) binder (0.5 ml) to form a thick paste. The binder was prepared by dissolving 1% PVA solution. Then, the mixture of sample and binder were placed in a mould (10 mm diameter and 1.5 mm thickness) and pressed in a hydraulic press with a uniaxial pressure of 25 MPa [8]. Similarly, the sensor pellets, MAC0.07 and MAC0.14, were prepared and all the samples were heated at 400 K for 15 h.

2.4 *Gas sensor chamber design*

The gas detection system has been described in the previous studies [8]. Briefly, one of the sensor sample pellets was clamped between two clamps to calculate the sensing reaction, as shown in figure 1f. The ends of the clamps were connected to an electrode cable and inserted inside the upper lead opening of the sensing chamber. The lead opening was sealed with a rubber cork. One of the two cables acted as a cathode, whereas the other acted as an anode. The other two ends of the electrode cables were connected to the source measurement unit (the digital micro-ohmmeter), which was used to extract the value of resistance, R_g, of the sensor samples on the passage of O_2 and CO. The range of the current source used for calculating was 0–50 mA. The voltage produced across the contact resistance depends on the flow of charges between the two contact leads. In turn, the flow of charge, between the contact points, depends on the change in resistance owing to the absorption of gas on the surface of the contact material.

Initially, argon gas was allowed to pass through the inlet valve of the sensing chamber. Then, the sensor sample (e.g., MAC0.07) was exposed to O_2 at 300 K with a relative humidity (RH) of 37%. The resistance, R_g, between the two electrodes of the sensor sample was calculated as a function of time and R_a being the instantaneous value of the sensor resistance. In the processing unit, the produced voltage signal V_{out} across the sensor element is the output across contacts 2 and 3. In the display unit, the electrodes from contacts 2 and 3 are connected to the LCR Q metre to measure resistance and then to calculate the response of the sensor. The gas sensors work on the principle that on adsorption of the gas molecules on the surface of a semiconductor, there is a change in the electrical resistance on the sensor surface due to large specific surface area and increased O_2 adsorption sites [6]. The gas–solid interaction affects the resistance of the material because of the density of electronic charges on the surface.

The different operating temperatures (300, 400 and 500 K) were maintained by placing a hot metal electrode-coated heating plate/pad (supplied with voltage of 12 V and current of 1 A) below the sample. It was observed that at higher temperatures like above 500 K, there was a rise in electrical disturbance on the surface. This disturbance hindered the sensor activity and hence, the response dropped. Therefore, the optimum temperature (300–500 K) was revealed in the present gas sensing approach [6].

3. Results and discussion

3.1 *Structural analysis*

The XRD pattern of MA, MAC0.07 and MAC0.14 are shown in figure 2. In the figure, the samples of MAC0.07 and MAC0.14 show that the observed diffraction peaks are indexed to cubic phase (00-001-115) with $a = 8.433$ Å for $MgAl_2O_4$. The crystalline phase of MA shows well-defined and high-intensity major peaks at diffraction angle $2\theta = 29.39°$, $30.93°$, $36.81°$, $42.80°$, $51°$ and $62.12°$ with planes (111), (220), (311), (400), (211) and (440), respectively, which match the standard data correlated with the JCPDS File No. 21152 (cubical crystal structure with face-centred lattice). The presence of $MgAl_2O_4$ is proved by the predominant diffraction peaks of MAC sample observed at $2\theta = 36.24°$, $43.45°$, $52.64°$, $57.51°$ and $68.28°$. In addition, the presence of ceria is marked by the diffraction peaks at $2\theta = 28.64°$, $57.45°$, $76.95°$, $80.81°$ and $89.11°$.

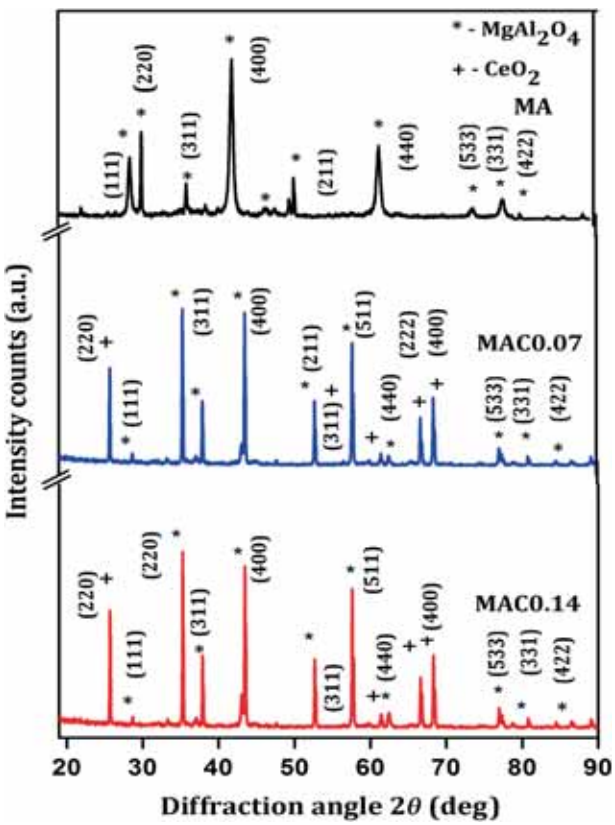

Figure 2. XRD pattern of the samples MA, MAC0.07 and MAC0.14.

Table 1. Elemental composition of CeO_2 and $MgAl_2O_4$ composites' powder sample.

Sample	XRD, crystalline size, D (nm)	EDAX (± 0.01 wt%)				UV–Vis	
		Mg	Al	O	Ce	Wavelength, λ (nm)	Bandgap, E_g (eV)
MA	40	33.91	8.84	57.25	—	358	3.46
MAC0.07	80	12.17	25.24	62.52	0.07	372	3.33
MAC0.14	83	18.26	20.36	61.24	0.14	375	3.30

For the prepared samples, the obtained diffraction peaks are sharp because of the grain growth of crystalline structure even at 1130 K. The diffraction peaks of MgO and Al_2O_3 decreased, whereas spinel peaks of $MgAl_2O_4$ were observed clearly in the X-ray spectra for the samples. Using Scherer's formula ($D = (0.9 * \lambda)/(\beta * \cos\theta)$; θ = angle between the incident ray and the scattering planes; λ = wavelength of X-ray; β = full-width at half-maximum), the average crystalline size of composite samples for all the major diffraction peaks are conferred in table 1. The average crystalline sizes calculated are 40, 80 and 82 nm for MA, MAC0.07 and MAC0.14, respectively [13,15,23].

3.2 *Functional groups' studies*

The FTIR spectra recorded for samples MA, MAC0.07 and MAC0.14 in the range of 4000–400 cm^{-1} are shown in figure 3. The band observed at 1625 cm^{-1} is attributed to the bending mode of H–O–H vibrations. Some sharp and distinct bands observed at approximately 900 and 530 cm^{-1} indicate the presence of $MgAl_2O_4$. These bands correspond to the AlO_6 group and MgO_4 stretching, which helps in the formation of $MgAl_2O_4$ spinel. Generally, the cubic ceria structure possesses six optical–phonon branches, but only one vibration at a band recorded at 480 cm^{-1} (symmetric breathing of the O_2 ions around Ce ions) is generally detected by the FTIR spectral measurements. The small variations noted in the band at approximately 730–530 cm^{-1} are owing to the addition of CeO_2 to $MgAl_2O_4$. Some sharp and distinct bends observed at approximately 1000 and 1500 cm^{-1} indicate small amounts of acetates and ethoxide. Thus, FTIR results show the presence of CeO_2 and $MgAl_2O_4$, synthesized by the chemical diffusion reaction in the presence of a molten salt [20,21].

3.3 *Thermal analysis*

The TGA and DTA are performed at 10°C min^{-1} in static air. Figure 4 shows the TGA (thermal decomposition and dissociation) reactions involved during the MSS process. An endothermic reaction was observed in the composite samples, at 410 K, owing to dehydration of the water molecules present in the samples. At 410 K, approximately 1.24% weight loss was observed in MAC. It was observed that beyond 573 K there was a minor change in the weight loss of the compound

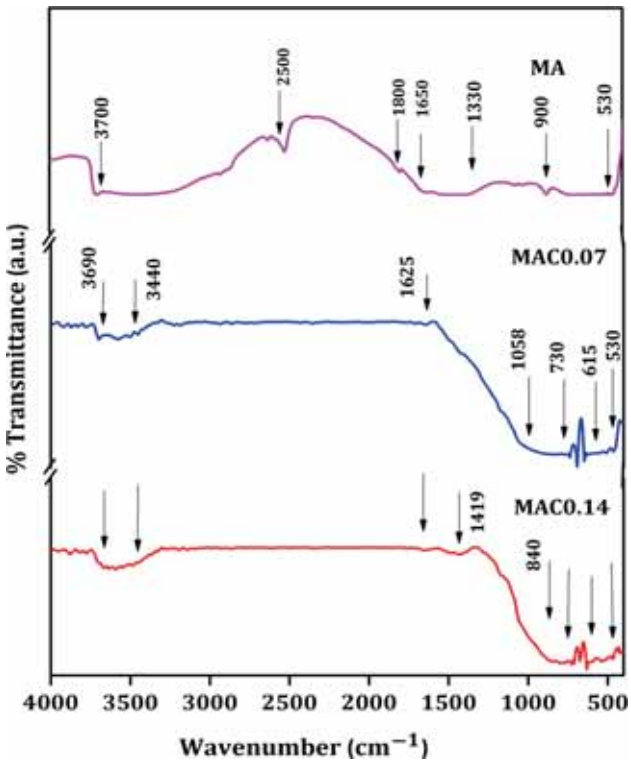

Figure 3. FTIR spectra of the samples MA, MAC0.07 and MAC0.14.

and the same stabilized around 890 K. Therefore, beyond this temperature the compound completely transforms into a single-phase crystalline structure.

On analysing the DTA curve (figure 4), it is clear that there are exothermic peaks at 495 and 620 K owing to the partial decomposition of reactants such as MgO, Al_2O_3 and CeO_2 in the presence of NaCl–KCl flux. The transformation starts and produces a single-phase/foreign-phase CeO_2 and $MgAl_2O_4$ at this temperature. In addition, beyond 949 K, the complete transformation of the precursor into a single composite of CeO_2 and $MgAl_2O_4$ is observed [17,20] (figure 4).

3.4 *Surface morphological and ultrasonic studies*

Figure 5 shows SEM/EDAX spectra images of MA, MAC0.07 and MAC0.14. The scanning electron microscope image

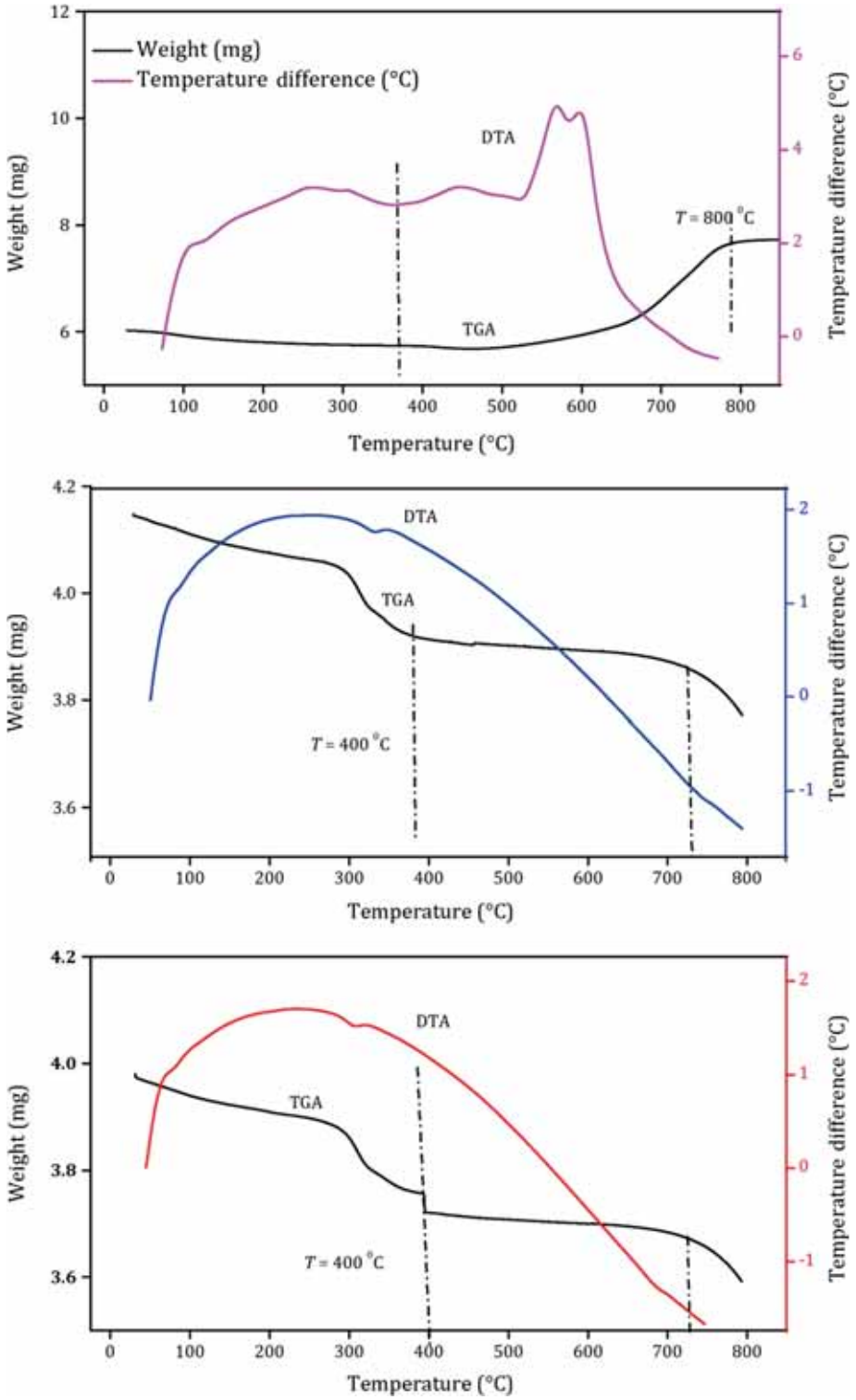

Figure 4. TGA–DTA profiles of the samples MA, MAC0.07 and MAC0.14.

shows that the particles are homogeneous in nature with minimum agglomeration. The energy-dispersive X-ray analysis profile shows that the concentrations of Mg, Al, Ce and O ions are in an approximate stoichiometry in the synthesized compound. The elemental analysis data of the samples and UV–Vis spectra of MA, MAC0.07 and MAC0.14 are presented in table 1. A broad absorption band at 358, 372 and 375 nm in the UV spectra for MA, MAC0.07

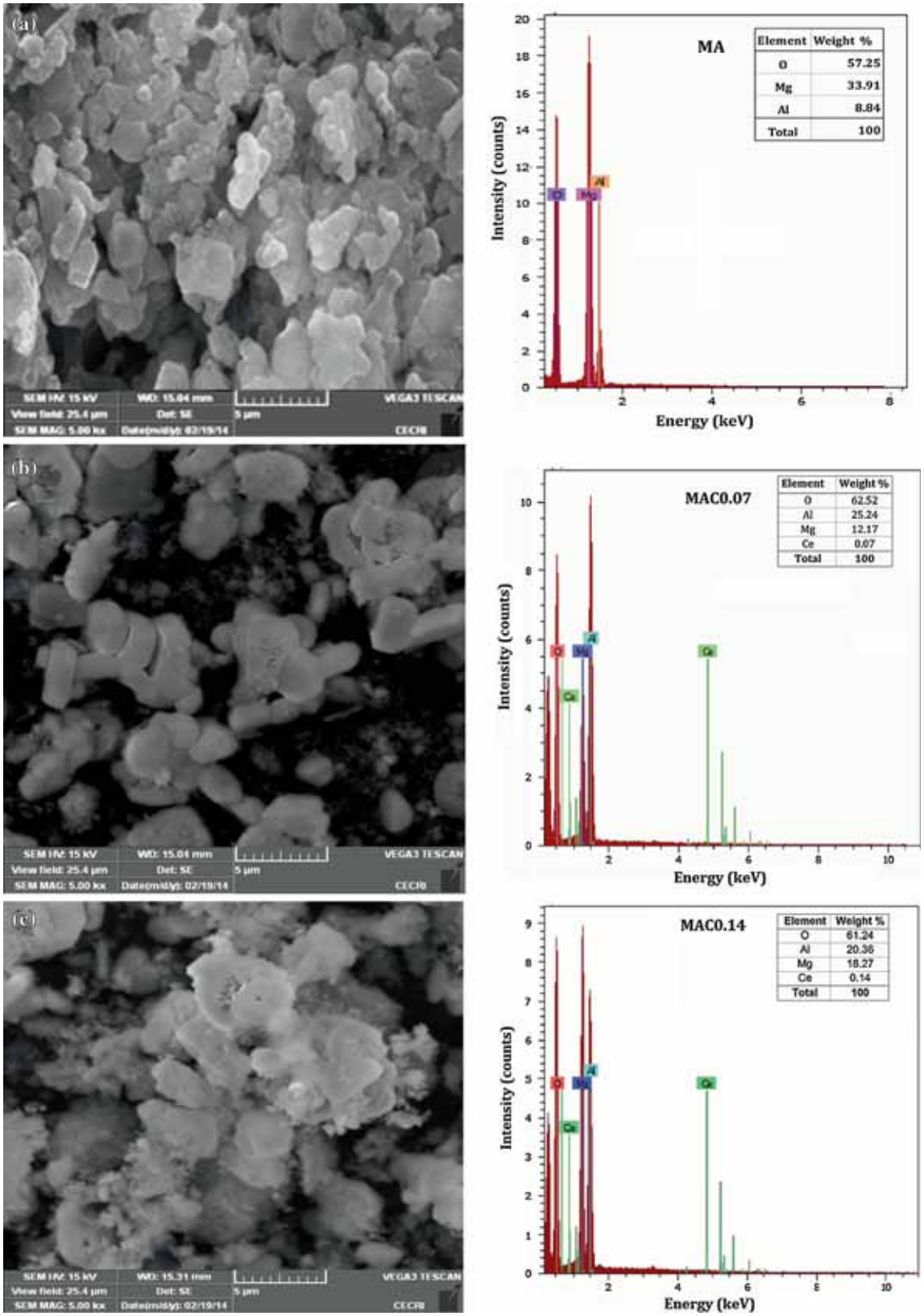

Figure 5. SEM image and EDAX pattern of the samples: (**a**) MA, (**b**) MAC0.07 and (**c**) MAC0.14.

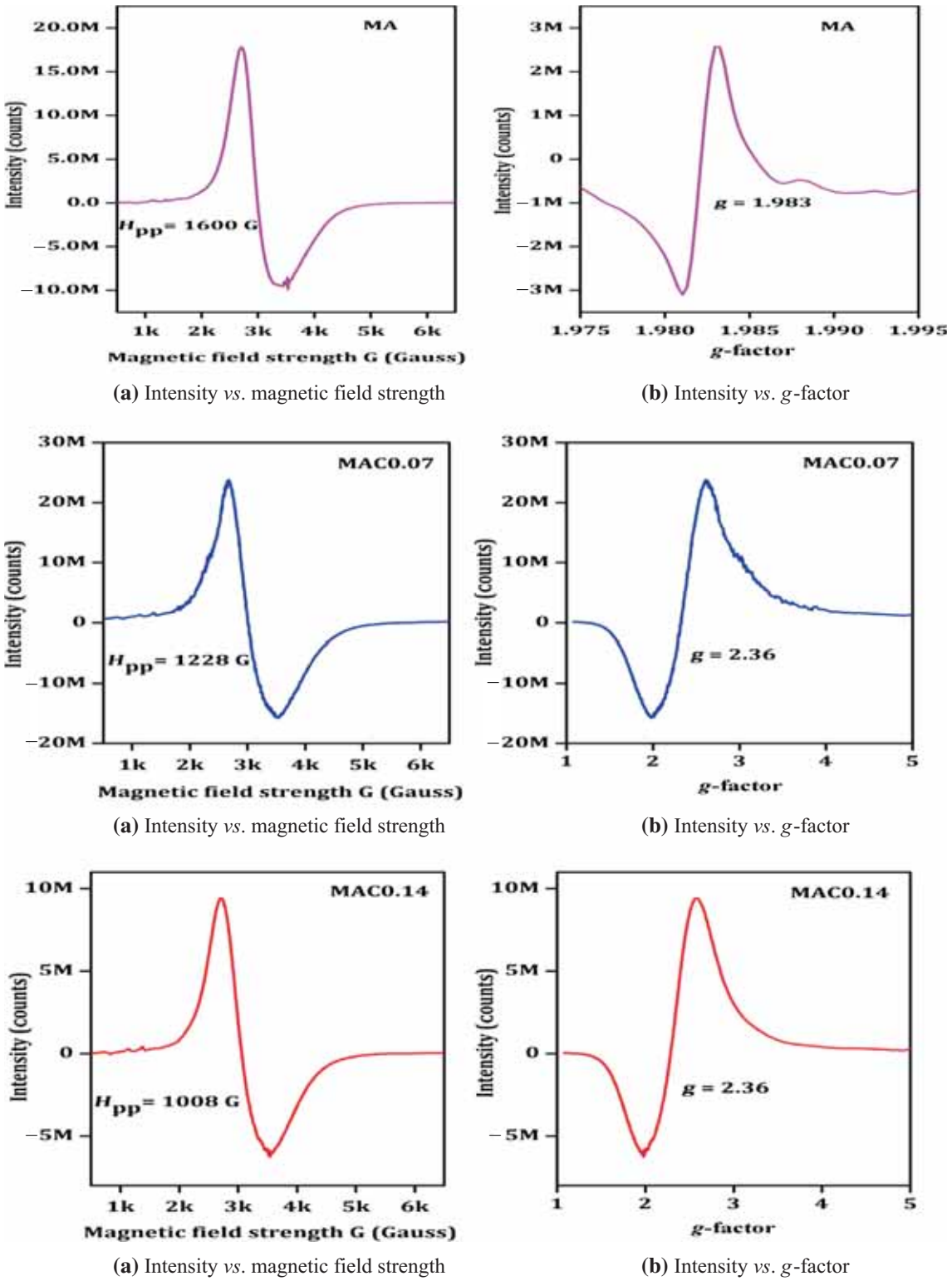

(a) Intensity *vs*. magnetic field strength **(b)** Intensity *vs*. g-factor

(a) Intensity *vs*. magnetic field strength **(b)** Intensity *vs*. g-factor

(a) Intensity *vs*. magnetic field strength **(b)** Intensity *vs*. g-factor

Figure 6. EPR spectra of the samples MA, MAC0.07 and MAC0.14.

and MAC0.14, respectively, indicates the absorbance of the samples. From the spectrum, the band gap energy of the material is determined using the equation $E_g = hv$. The E_g observed for the sensor sample is 3.45, 3.33 and 3.30 eV for MA, MAC0.07 and MAC0.14, respectively [20, 24,25].

3.5 *Paramagnetic analysis*

The paramagnetic resonance spectra of MA, MAC0.07 and MAC0.14 are provided in figure 6. It is reported that magnetization value, which reduces after the addition with Ce ions, plays a dominant role in the evaluation of resonance field and line widths. The EPR spectral studies of MA and composite of CeO_2 and $MgAl_2O_4$ are conducted to analyse their magnetic properties. The spectrum shows a single broad resonance peak. It is found that the value of peak-to-peak line width (H_{pp}) is reduced from 1505 to 1228 G after the addition of Ce ions. On further increase in the quantity of Ce concentration ($x = 0.14$), the H_{pp} value declines to a minimum of approximately 1008 G. The sample corresponding to MAC0.14 shows minimum g-value of 2.36 and resonance field (H_r) value of 1228 G [20,21]. Reduction in line width of composite samples is because of decrease in magnetic dipolar interaction and particle size. At a high frequency region, small value of line width is useful, as it reduces the eddy current losses.

High magnetization for the $MgAl_2O_4$ sample ($g = 1.98$) indicates high internal magnetic field (H_r) and resonance occurring at a low magnetic field. As the quantity of concentration increases, the g-value and the rate of magnetization also increases. Therefore, the H_r decreases. Consequently, for an increase in the quantity of concentration of 0.07 g of Ce, the resonance field decreases owing to the reduction in porosity. Thus, it is identified that a high nuclei is necessary to obtain powder reactant particles. To form a crystalline state, the surface of the reactant particles is used as the nucleation site [20,26]. The reactant particles nucleate heterogeneously on the surfaces of the nearby crystals and form an agglomerated fine sample of CeO_2 and $MgAl_2O_4$.

3.6 *O_2 gas response analysis*

The gas sensing process of the samples works on the receptor, interface and transducer mechanism. Initially, the receptor mechanism involves the identification of O_2 as target gas in the surface of the prepared sample. This is followed by the interaction of O_2 with the sample surface. Next, an interface mechanism produces an electronic change in the oxide surface of the sample that is converted into an electrical resistance in transducer mechanism. This is towing to the free electron flow through the grain boundaries of the sample inducing electronic changes [6,25,27].

This sample acts as an electrical resistor in the variation of O_2 concentration levels and in the operating temperature. Therefore, the transferring of electrons is done from the surface of metal oxide to the O_2, as shown in the following equations (1–3):

$$O_{2(gas)} = O_{2(ads)} = O^-_{2(ads)} = O^-_{(ads)} \quad (1)$$

$$O^-_{(ads)} O^{2-}_{(ads)} = O^{2-} \quad (2)$$

$$\text{Sensor response } (S_{O_2}) = \frac{(R_g - R_a)}{R_a} \quad (3)$$

During the adsorption process, O_2 gas adsorbed on the surface is mainly in the form of O_2^- below the transition operating temperature and O_2 dominates in the form of O^- and O^{2-} above this temperature. As the operating temperature increases, the baseline resistance (R_a) tends to decrease because of the behaviour of nanoparticles. Similarly, the reaction of a reducing gas (CO) decreases the original resistance of the sensor sample [6,7,27].

The relationship between RH and the sensing response of all the samples with different concentration levels of O_2 were also investigated. For constant pressure of O_2 at different operating temperatures, its RH decreased from 60 to 37% RH in 30 s. However, it was observed that all the samples established, approximately, a similar RH% on the passage of the O_2 at different operating temperatures. Below 37% of RH, the response value gets decreased and the humidity exerted a negative effect on the gas sensing response of the sensor sample [16,17,28]. The pellet thickness of MAC0.07 (3.1 mm) and MAC0.14 (3.15 mm) increased from 3 mm on the passage of O_2. However, for MA (2.95 mm), the pellet thickness slightly decreases on the passage of O_2 owing to the interaction of the porous structure with the sensing gas. Moreover, within three cycles of repeatability, the sensor sample still maintained a good response and recovery state.

The layer of charged O_2, at the surface, repels other electrons from interacting with the sample, creating an electron depletion region. At the grain boundaries, this results in an increased potential barrier. This increased potential barrier slows down the flow of electrons across the surface and increases electrical resistance. Each time argon gas was fed continuously into the sensing chamber prior to the sensing process. On every occasion, the gas sensing chamber was cleaned with a vacuum pump before exposure of argon and, subsequently, the passage of O_2 to the chamber. The minimum temperature, at which the baseline resistance of the samples was measured, was 300 K. The resistance of the sensor increased in the presence of O_2 and recovered on the passage of argon gas.

In addition, the sensing measurements were individually recorded and repeated uniformly at an interval in MA and MAC0.14. The results were taken at 120 s time interval to allow the sensor to regain its baseline resistance value. In addition, this O_2 vacancy formation in CeO_2 addition (MAC0.07) resulted in partial reduction in the material surface. At operating temperatures above 300 K, O_2 was chemisorbed in the form of O_2^-, in both pure and composite sensors, leading to an increase in the sensor resistance. This serves as a reason, in which O_2^- species are bound at the vicinity of O_2 vacancies in the sensor surface.

The resistance and sensor response of MA, MAC0.07 and MAC0.14 at different pressures (0.5, 1.0 and 1.5 bar) of O_2 at different operating temperatures (300, 400 and 500 K) are shown in figure 7. Generally, it takes 20 s to fill

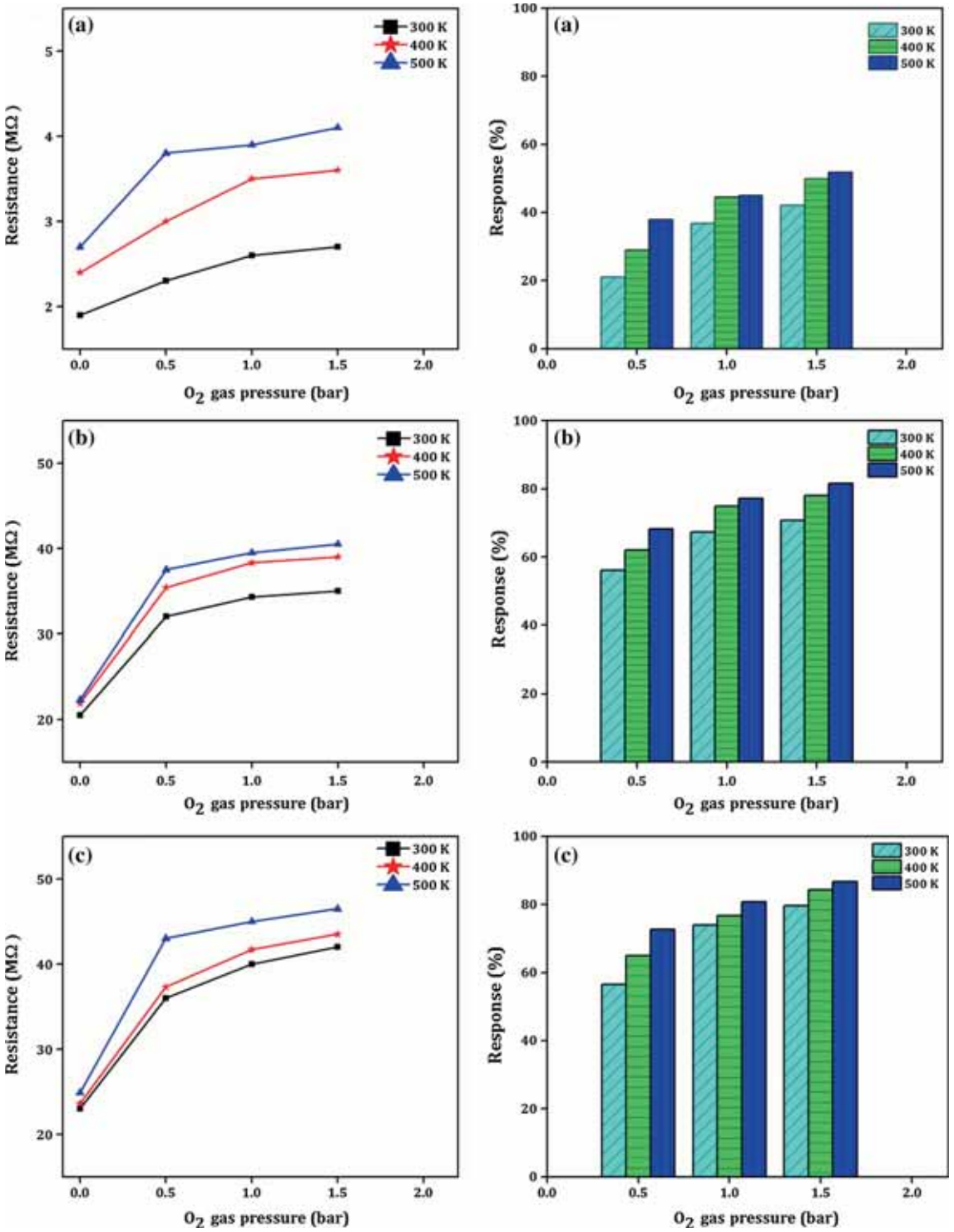

Figure 7. Resistance and sensor response of the samples: (**a**) MA, (**b**) MAC0.07 and (**c**) MAC0.14 at different pressures and different operating temperatures of oxygen gas.

the mixer chamber in the gas sensor setup, 60 s to react with sample surface and 20 s to evacuate the sensing gas from the chamber. At higher temperatures, O^- and O^{2-} ions exist as major species causing a redox reaction of the composite sensor surface. The gas sensing ability and reproducibility of the samples were tested by repeating the earlier experiments for different concentrations of sensing gases to three cycles. In addition, a similar experimental procedure was repeated for CO separately in the sensing chamber.

Table 2. Response and recovery time of CeO_2 and $MgAl_2O_4$ composites' sensor sample for sensing of O_2, CO and ethanol gas.

		Sensor response (%) at operating temperature (K)			Response time (s) at operating temperature (K)			Recovery time (s) at operating temperature (K)		
Sample	Pressure of O_2 gas (bar)	300	400	500	300	400	500	300	400	500
O_2 gas										
MA	0.5	21	29	52	50	45	41	61	60	57
	1.0	37	45	45	40	39	35	56	54	51
	1.5	42	50	52	38	37	33	51	49	46
MAC0.07	0.5	56	62	68	47	45	40	58	56	53
	1.0	67	75	77	38	35	31	54	51	48
	1.5	71	78	82	35	33	29	51	47	44
MAC0.14	0.5	57	65	73	45	43	37	56	55	52
	1.0	74	77	81	35	33	29	50	48	45
	1.5	80	84	87	33	30	28	48	45	42
CO gas										
MA	0.5	11	38	48	52	48	45	64	61	60
	1.0	11	38	48	42	41	37	58	56	53
	1.5	21	42	52	40	39	35	53	51	48
MAC0.07	0.5	64	69	71	49	47	42	60	58	55
	1.0	71	75	77	40	37	35	56	53	50
	1.5	75	79	81	37	35	30	53	49	46
MAC0.14	0.5	72	75	80	47	45	39	58	57	54
	1.0	77	79	83	37	35	31	52	50	47
	1.5	78	81	85	35	32	30	50	47	44
Ethanol gas										
MA	50 ppm	50	26	46	48	55	52	50	65	62
	100 ppm	100	42	58	52	50	50	48	64	60
MAC0.07	50 ppm	50	27	55	76	45	43	40	60	58
	100 ppm	100	51	83	89	44	40	38	58	55
MAC0.14	50 ppm	50	35	61	77	43	40	38	55	55
	100 ppm	100	52	84	89	42	38	35	53	51

As the number of O^{2-} ions getting adsorbed on the surface increases, in turn the sample resistance increases. This leads to an increase in the sample resistance in the presence of O_2 at different operating temperatures [29]. The resistance values of the sensor samples are 35, 39 and 41MΩ with the pressure of 1.5 bar on the passage of O_2 at different operating temperatures, namely, 300, 400 and 500 K, respectively, for MAC0.07. Similarly, the resistance values were 42, 44 and 47 MΩ at 300, 400 and 500 K, respectively, for O_2 with the pressure of 1.5 bar for MAC0.14. The percentages of increase in O_2 resistance (R_g) values on increasing the temperature from 300 to 500 K for MAC0.07 at 0.5, 1.0 and 1.5 bar are 18, 17 and 17%, respectively. Similarly, the percentages of increase in O_2 resistance values on increasing the temperature from 300 to 500 K for the sample MAC0.14 at 0.5, 1.0 and 1.5 bar are 19.4, 12.5 and 11.9%, respectively. In addition, the response of 87% was attained for the sample MAC0.14 at an operating temperature of 500 K with 1.5 bar O_2 pressure.

Furthermore, table 2 shows that at 500 K a good recovery property is gained for all the samples in O_2, even when compared with the other operating temperatures, namely, 300 and 400 K. At the same time, at 500 K, a linear steady variation in response was observed while increasing the O_2 concentration for all samples. This change reduced the defects of O_2 vacancies, which provided abundant local donor energy levels in the composite sensor with a decreased charge carrier concentration. On removing O_2, the reduction of the lattice cannot occur quickly; hence, time is taken (recovery time) by the sensor to regain its original conductivity.

3.7 *CO gas response analysis*

Initially, the clean dry air was passed through the inlet valve to remove the organic remains inside the chamber. Then, air resistance, R_a, was noted across the sample (e.g., MAC0.07). Finally, CO (target gas) was passed through the inlet valve

of the sensing chamber and the inlet valve was closed. The sample was allowed for reacting with the gas for 3 min, resulting in a reaction on the surface of the sensor sample. The gas concentration inside the chamber was maintained by adjusting the flow rate using a mass flow controller (0–500 slpm; 140 Ultra-Low ΔP Mass Flow Controllers; SmartTrak, L Monterey, CA). Thus, a potential difference ($V_a - V_b$) was noted across the sensor sample surface and hence, the gas resistance (R_g) was decreased [25,30,31]. This decrease in R_g across the gas sensor sample was calculated by a voltage drop technique. After exhausting the existing gas in the chamber, the chamber was evacuated using an external rotary vacuum pump after which the clean dry air was passed into the inlet valve.

Next, CO was allowed through the inlet valve. The same procedure was repeated several times to calculate an average value of reproducibility in the sensor response of the samples. In addition, the pressure of CO was also changed at different levels ($P = 0.5$ to 1.5 bar) by conducting different tests. Thus, the similar experimental procedure was used to measure the gas sensor response of all samples. The sensor response for CO was calculated using the following equations (4–6), when $R_a > R_g$:

$$O_{2(air)} + 2e^- = O^-_{(ads)} \tag{4}$$

$$CO + O^-_{(ads)} = CO_2 + e^- \tag{5}$$

$$\text{Sensor response } (S_{CO}) = \frac{(R_a - R_g)}{R_a} \tag{6}$$

where, R_g is the change in resistance of the sensor in the presence of CO and R_a and the resistance of the sensor in the presence of dry air. The change in resistance was calculated by the readout from the electrodes using a digital ohmmeter. An increase in the calcination temperature in turn increases the crystallization of all the samples, but an increase in the dopant addition alters the concentration of O_2 vacancies. The substitution of CeO_2 in MgO and Al_2O_3 creates O_2 vacancies and donates electrons to make it an n-type semiconductor.

The resistance and sensor response of MA, MAC0.07 and MAC0.14 at different pressures (0.5, 1.0 and 1.5 bar) of CO and at different operating temperatures (300, 400 and 500 K) are shown in figure 8. From the observation, it was noted that the response of the samples was found to increase at 400 K and remain almost constant at 500 K. This was because of the rate of the sensor surface reaction with target gases and the diffusion of the surface species. The resistance of the sample was found to decrease with an increase in the pressure of CO at room temperature. In addition, the resistance of CeO_2 added with $MgAl_2O_4$ at different temperatures was found to decrease further towards increasing CO concentrations. The percentage of CO resistance values on increasing the temperature from 300 to 500 K for MAC0.07 at 0.5, 1.0 and 1.5 bar are 10, 16 and 17% increase, respectively.

Similarly, the percentage of increase in O_2 resistance values on increasing temperature from 300 to 500 K for MAC0.14 at 0.5, 1.0 and 1.5 bar are 15, 20 and 30%, respectively. Thus, the sensor response and its response and recovery time are shown in table 2. Figures 8 and 9 depict that an increase in the concentration of CeO_2 leads to an increase in sensor response. Similarly with an increase in operating temperatures, conductivity of the sensor samples increases as well. The response of the sensor sample is reproducible, returning to the baseline value (resistance recovery) following successive output for O_2 and CO, as shown in table 2. The response plot shows that on increasing operating temperature from 300 to 500 K, the response and recovery time changes from 33 and 48 s, to 28 and 42 s, respectively, for MAC0.14 at 1.5 bar pressure. From these results, the good performance of MAC in terms of higher operating temperature with fast response and recovery time were noted.

3.8 *Ethanol gas response analysis*

The sensor response of nanoparticles for ethanol is calculated by the change in the surface resistance in the presence of gas, i.e., the ratio of surface resistance of the sample in air (R_a) and in ethanol (R_g). It is observed that as the operating temperature increases, the surface resistance decreases. The gas sensing mechanism of semiconductor metal oxide gas sensors is based on the absorption of target gas on the surface sites of the sample. The surface of MAC is covered with chemisorbed negative O_2 ion and it reacts with the β-H of C_2H_5OH. Thus, the surface resistance of MAC decreases. When MAC is exposed to air, an O_2 ion molecule is absorbed onto the surface of MAC to form the O^{2-} or O^- ion [18,32,33]. This is achieved by attracting an electron from the conduction band of the MAC surface as shown in the following equations (7, 8):

$$O_{2(air)} + 2e^- = O_2^{2-} \tag{7}$$

$$2O_{2(air)} + 1e^- = 2O^{2-} \tag{8}$$

Thus, the high resistance of MAC is noted in the passage of air. For active ethanol sensing at moderate temperature, the ethanol reacts with O_2 ion molecule on the surface and gives an electron as can be described by the following equations (9–11):

$$2C_2H_5OH + O_2^{2-} = 2CH_3CHO + 2H_2O + 2e^- \tag{9}$$

$$C_2H_5OH + O^{2-} = 2CH_3CHO + 2H_2O + 1e^- \tag{10}$$

$$\text{Sensor response } (S_{ethanol}) = \frac{\left(R_a - R_g\right)}{R_a} \tag{11}$$

The gas sensing mechanism depends on the surface reaction between chemisorbed O_2 ions and the reducing gases. The adsorption of O_2 on the sensor surface has two important forms: physisorption and chemisorption. The chemisorption

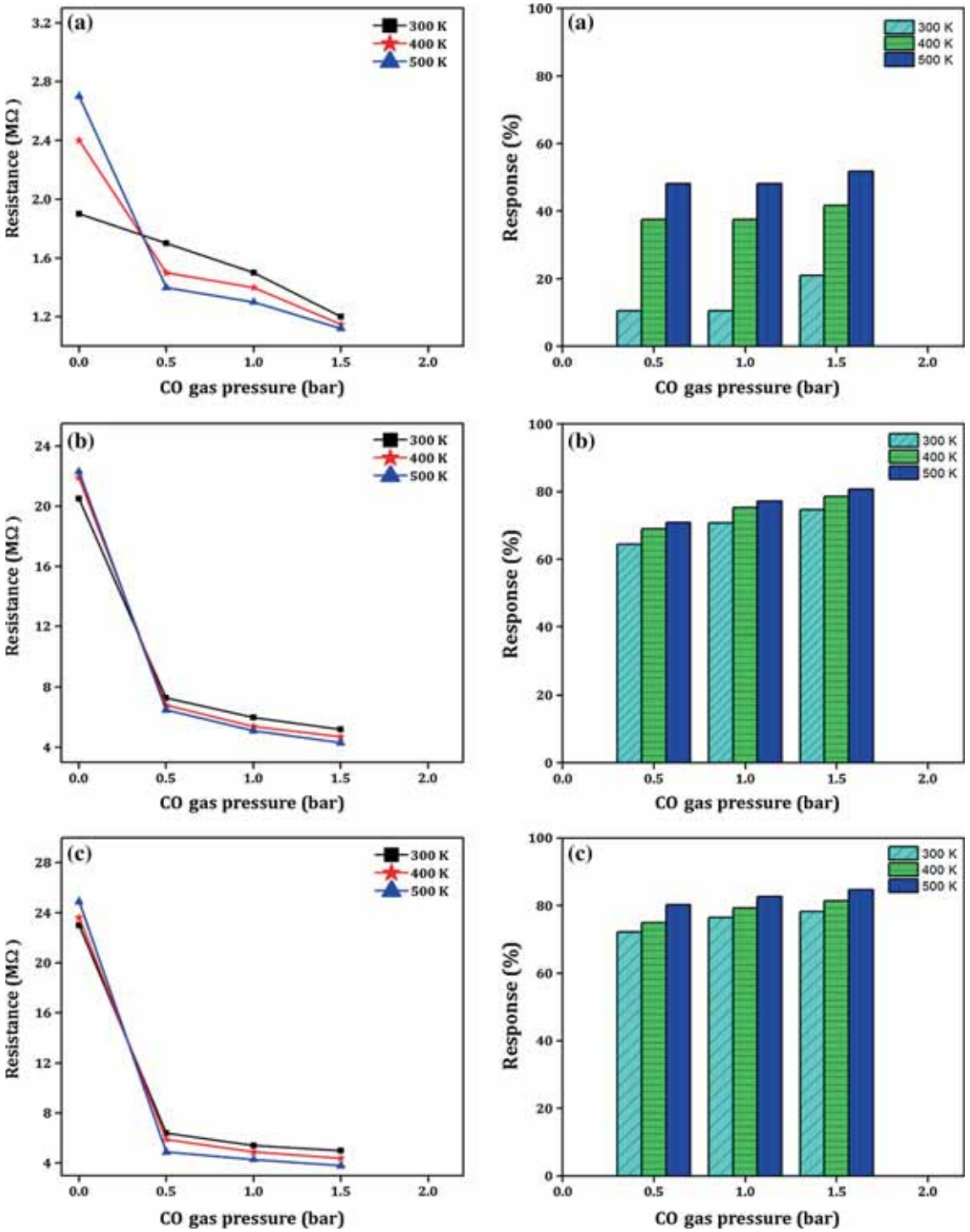

Figure 8. Resistance and sensor response of the samples (**a**) MA, (**b**) MAC0.07 and (**c**) MAC0.14 at different pressures and different operating temperatures of carbon monoxide gas.

process is dominant at an increased operating temperature. The transition from physisorption to chemisorption needs more activation energy (i.e., temperature), which can be accomplished by increasing the operating temperature. The gas sensor response of the samples on the passage of ethanol at concentrations of 50 and 100 ppm is shown in figure 9. It has been reported that the amount of O_2 adsorbed on the sensor surface goes on increasing with an increase in temperature, reaches a maximum level, and then decreases with further increase in the operating temperature.

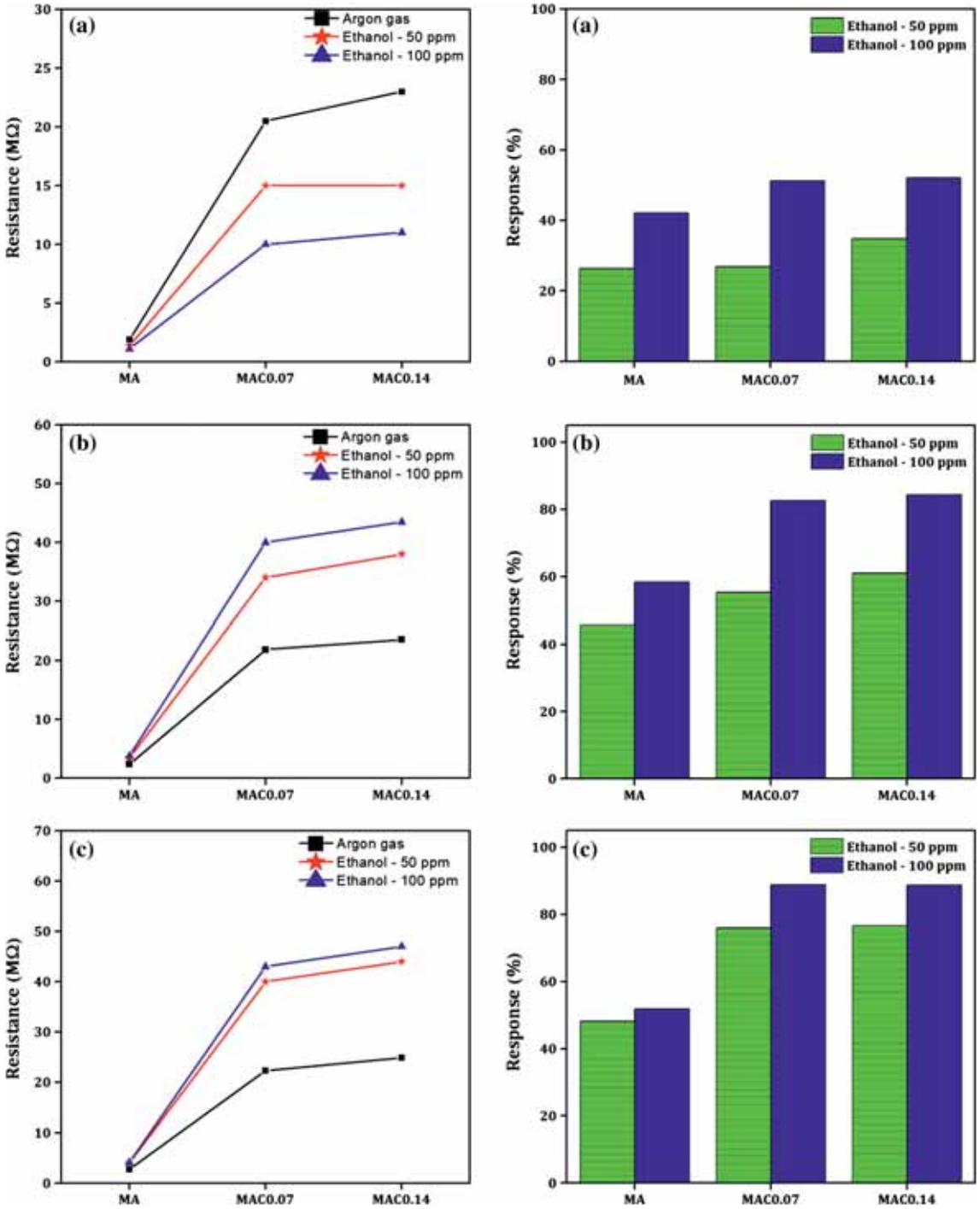

Figure 9. Resistance and sensor response of the samples MA, MAC0.07 and MAC0.14 at different concentrations and different operating temperatures (**a**) 300 K, (**b**) 400 K and (**c**) 500 K of ethanol gas.

The rate of oxidation is the function of the amount of adsorbed O_2 on the surface and the type of gas to be tested. In the larger oxidation, the number of electrons released would be more, and in turn, the larger would be their sensor response. The C–C and C–H bonds in the sample are quite strong owing to Van-der-Waals forces. Only at higher temperatures, the C–C and C–H bonds break resulting in carbon and hydrogen separation. The atmospheric O_2 gets adsorbed on the surface of the film. Thus, ethanol gets oxidized to CO_2 and H_2O and the electrons released from the surface reaction transfer back into the conduction band increasing the conductivity and lowering the resistance of MAC.

It is concluded that the number of available surface sites for adsorption start to decrease, leading to a decrease in the

electrical resistance of O_2, on reaching its maximum temperature (500 K). It is observed that the composites exhibit high response to 100 ppm of ethanol for MA (52%), MAC0.07 (89%) and MAC0.14 (89%) at 500 K as shown in table 2. These findings indicate that the gas-sensing performance is increased at different operating temperatures and on the increase in gas concentrations, which is assured because of the increase in concentration of CeO_2 with $MgAl_2O_4$ (0.07 and 0.14 g).

From all these reactions, it is observed that a huge number of electrons are released to the surface of the sensor substrate. This, in turn makes the surface barrier to decrease, with the depletion layer to be thinner. Thus, the electrical conductance in the surface increases. More gas is adsorbed by the surface and hence the gas sensitivity is enhanced. In addition, an increase in operating temperature causes oxidation of a large amount of gas molecules, thus producing a very large number of electrons. Therefore, conductivity increases to a large extent. This shows that the gas sensitivity increases with operating temperature. However, the sensitivity decreases at higher operating temperature greater than 550 K, as the O_2 adsorbants are desorbed from the surface of the sensor. In addition, at a higher operating temperature, the carrier concentration increases due to intrinsic thermal excitation.

Repeatability and stability measurements are important aspects in deciding the sensor performance. Furthermore, the long-term reproducibility of MA, MAC0.07 and MAC0.14 was determined by repeatedly noting its response over a period of 3 days. The observed results show that the composite of CeO_2 and $MgAl_2O_4$ acts as a potential candidate for gas sensing applications than their individual material as reported elsewhere [16,19]. In turn, selectivity, cross-sensitivity and humidity interference along with impurities were considered to be the future work of this investigation.

4. Conclusion

The resistive type of O_2 and CO sensors based on $MgAl_2O_4$ and CeO_2 were synthesized by the MSS method and fabricated by pelletization with electrodes placed on both ends. It was found that composites of CeO_2 and $MgAl_2O_4$ were capable of detecting even a small variation in concentration of O_2, CO and ethanol. The average crystallite size was 40, 80 and 83 nm for MA, MAC0.07 and MAC0.14, respectively. The existence of functional groups at 900 and 530 cm^{-1} corresponding to AlO_6 group, the lattice vibration of MgO_4 stretching and the observation of band approximately at 730–530 cm^{-1} were confirmed through FTIR studies for the presence of CeO_2. The TGA reactions involved during the MSS method showed an endothermic reaction observed at 410 K, owing to dehydration of the water molecules present in the synthesized compound. At this temperature, approximately, 1.24% weight loss was observed in the sample.

The results of SEM/EDAX studies confirmed spherical morphology with elemental composition Mg, Al, O and Ce. UV–Vis absorption spectra showed band gap energy (E_g) 3.45, 3.33 and 3.30 eV for the sensor samples. The EPR spectrum of MAC showed a much narrow signal centred at $g = 2.36$, indicating magnetic interactions of individual elements in the samples. The response of MAC0.07 increases at 11%, but that of MAC0.14 increases at 7% on increasing the operating temperatures from 300 to 500 K for O_2. Similarly, the response of MAC0.07 increases at 6%, but that of MAC0.14 increases at 7% on increasing the operating temperatures from 300 to 500 K for CO. This clearly indicates that a smaller concentration of CeO_2 doping is suitable for sensing both oxidizing and reducing gases. From this research, it is concluded that MAC0.14 possesses good resistance and high sensor response for O_2, CO and ethanol.

Acknowledgements

We are thankful to Dr L. John Berchmans in supporting us to carry out our research successfully in Electro-Pyrometallurgy Division, CSIR—Central Electrochemical Research Institute, Karaikudi 630006, India.

References

[1] Jimenez-Cadena G, Riu J and Rius F X 2007 *Analyst* **132** 1083
[2] Takada T, Fukunaga T and Maekawa T 2000 *Sens. Actuators B Chem*. **66** 22
[3] Korotcenkov G 2007 *Mater. Sci. Eng. B* **139** 1
[4] Barsan N and Weimar U 2001 *J. Electroceram.* **7** 143
[5] Di Francia G, Alfano B and La Ferrara V 2009 *J. Sens.* **2009** 1
[6] Liu X, Cheng S, Liu H, Hu S, Zhang D and Ning H 2012 *Sensors* **12** 9635
[7] Tao J and Batzill M (eds) 2013 *Metal oxide nanomaterials for chemical sensors* (Springer: Berlin) p 35
[8] Nithyavathy N, Arunmetha S, Dhineshbabu N and Rajendran V 2015 *J. Nanosci. Nanotechnol*. **15** 5112
[9] Kurien S, Sebastian S, Mathew J and George K 2004 *Indian J. Pure Appl. Phys*. **42** 926
[10] Rufner J, Anderson D, Benthem and Castro R H 2013 *J. Am. Ceram. Soc.* **96** 2077
[11] Ping L R, Azad A M and Dung T W 2001 *Mater. Res. Bull.* **36** 1417
[12] Surendran K, Bijumon P, Mohanan P and Sebastian M 2005 *Appl. Phys. A* **81** 823
[13] Laobuthee A, Koonsaeng N, Ksapabutr B, Panapoy M and Veranitisagul C 2005 *Int. J. Mater. Struct. Reliab*. **3** 95
[14] Ganesh I, Olhero S M, Rebelo A H and Ferreira J 2008 *J. Am. Ceram. Soc*. **91** 1905
[15] Lee P Y, Suematsu H, Yano T and Yatsui K 2006 *J. Nanopart. Res*. **8** 91
[16] Jasinski P, Suzuki T and Anderson H U 2003 *Sens. Actuators B. Chem.* **95** 73
[17] Izu N, Shin W and Murayama N 2003 *Sens. Actuators B Chem*. **93** 449
[18] Kumar K L A, Durgajanani S, Jeyaprakash B G and Rayappan J B B 2013 *Sens. Actuators B Chem.* **177** 19
[19] Izu N, Matsubara I, Itoh T, Akamatsu T and Shin W 2013 *Sensors* **13** 3252

[20] Tabaza W, Swart H and Kroon R 2014 *Physica B Condens. Matter* **439** 109
[21] Martos M, Julián-Łópez B, Folgado J V, Cordoncillo E and Escribano P 2008 *Euro. J. Inorg. Chem*. **2008** 3163
[22] Durrani S, Al-Kuhaili M F, Bakhtiari I A and Haider M B 2012 *Sensors* **12** 2598
[23] Arockiam S I, Regis A P P and Berchmans L J 2012 *Synthesis* **4** 798
[24] Jiang X, Lou L, Chen Y and Zheng X 2004 *Catal. Lett*. **94** 49
[25] Rashad M, Zaki Z and El-Shall H 2009 *J. Mater. Sci*. **44** 2992
[26] Kale M, Joshi C and Moharil S 2014 *Int. J. Res. Advent. Technol*. **2** 342
[27] Batzill and Diebold U 2007 *Phys. Chem. Chem. Phys*. **9** 2307
[28] Moos R, Izu N, Rettig F, Reiß S, Shin W and Matsubara I 2011 *Sensors* **11** 3439
[29] Nithyavathy N, Arunmetha S, Vinoth M, Sriram G and Rajendran V 2016 *J. Electron. Mater.* **45** 2193
[30] Bai H and Shi G 2007 *Sensors* **7** 267
[31] Birkefeld L D, Azad A M and Akbar S A 1992 *J. Am. Ceram. Soc*. **75** 2964
[32] Johari A, Rana V and Chander Bhatnagar M 2011 *Nanomater. Nanotechnol*. **1** 49
[33] Zoolfakar A S, Ahmad M Z, Rani R A, Ou J Z, Balendhran S, Zhuiykov S *et al* 2013 *Sens. Actuators B Chem*. **185** 620